

High Precision K -Shell Photoabsorption Cross Sections for Atomic Oxygen: Experiment and Theory

B. M. McLaughlin^{1,2}

¹*Centre for Theoretical Atomic, Molecular and Optical Physics (CTAMOP)
School of Mathematics and Physics, Queen's University Belfast
Belfast BT7 1NN, Northern Ireland, UK*

²*Institute for Theoretical Atomic and Molecular Physics (ITAMP)
Harvard Smithsonian Center for Astrophysics
MS-14, Cambridge, MA 02138, USA*

`b.mclaughlin@qub.ac.uk`

C. P. Ballance³

³*Department of Physics, 206 Allison Laboratory
Auburn University, Auburn, Alabama 36849-5311, USA*

`ballance@physics.auburn.edu`

K. P. Bowen⁴ and D. J. Gardenghi⁴

⁴*Department of Chemistry, University of Nevada
Las Vegas, Nevada 89154-4003, USA*

`bowenk4@gmail.com, dgardenghi@gmail.com`

W. C. Stolte^{4,5,6}

⁴*Department of Chemistry, University of Nevada
Las Vegas, Nevada 89154-4003, USA*

⁵*Harry Reid Center for Environmental Studies, University of Nevada
Las Vegas, Nevada 89154-4009 USA*

⁶*Advanced Light Source, Lawrence Berkeley National Laboratory
Berkeley, California 94720, USA*

`wcstolte@lbl.gov`

ABSTRACT

Photoabsorption of atomic oxygen in the energy region below the $1s^{-1}$ threshold in x-ray spectroscopy from *Chandra* and *XMM-Newton* is observed in a variety of x-ray binary spectra. Photoabsorption cross sections determined from an R-matrix method with pseudo-states (RMPS) and new, high precision measurements from the Advanced Light Source (ALS) are presented. High-resolution spectroscopy with $E/\Delta E \approx 4,250 \pm 400$ was obtained for photon energies from 520 eV to 555 eV at an energy resolution of 124 ± 12 meV FWHM. K -shell photoabsorption cross-section measurements were made with a re-analysis of previous experimental data on atomic oxygen at the ALS. Natural linewidths Γ are extracted for the $1s^{-1}2s^22p^4(^4P)np\ ^3P^\circ$ and $1s^{-1}2s^22p^4(^2P)np\ ^3P^\circ$ Rydberg resonances series and compared with theoretical predictions. Accurate cross sections and linewidths are obtained for applications in x-ray astronomy. Excellent agreement between theory and the ALS measurements is shown which will have profound implications for the modelling of x-ray spectra and spectral diagnostics.

Subject headings: photoabsorption, cross sections, inner shell, oxygen, x-ray binaries

1. Introduction

The photoionization process is one of the important radiative feedback processes in astrophysics (Miyake et al. 2010; Stancil et al. 2010). The increase in pressure caused by photoionization can trigger strong dynamic effects, such as photoionization hydrodynamics. The challenge in combining hydrodynamics with photoionization lies in the difference in time scales between the two process. Photoionization (PI) and photoabsorption (PA) processes play important roles in many physical systems, including a broad range of astrophysical objects as diverse as quasi-stellar objects (QSOs), the atmosphere of hot stars, protoplanetary nebula, HII regions, novae and supernovae. The *Chandra* and *XMM-Newton* satellites currently provides an abundance of x-ray spectra from astronomical objects; high-quality atomic data is needed to interpret such spectra (McLaughlin 2001; Mueller et al. 2010; Sant’Anna et al. 2011; Foster et al. 2010; Gharaibeh et al. 2011; McLaughlin & Ballance 2013). Theoretical studies, recently made on atomic carbon and it ions indicated high quality atomic data are necessary to accurately model *Chandra* observations in the x-ray spectrum of the blazar Mkn 421 (Hasoglu et al. 2010; Gharaibeh et al. 2011).

In the soft x-ray region (5-45 Å), spectroscopy, including *K*-shell transitions for atomic elements such as, C, N, O, Ne, S and Si, in neutral, or low stages of ionization and *L*-shell transitions of Fe and Ni, are a valuable tool for probing the extreme environments in active galactic nuclei (AGN’s), x-ray binary systems, cataclysmic variable stars (CV’s) and Wolf-Rayet Stars (McLaughlin 2001; Garcia et al. 2009; Foster et al. 2010; Skinner et al. 2010; Mueller et al. 2010; Gharaibeh et al. 2011; Sant’Anna et al. 2011), and the ISM (Garcia et al. 2011; Gharaibeh et al. 2011). Interstellar oxygen is found in both gas and dust phases, although the exact molecular form of the dust remains unknown. Therefore an accurate understanding of the gas phase constituents is necessary in order to measure the residual molecular and solid-phase components (Costantini et al. 2012).

In the x-ray community, Electron-Beam-Ion-Trap (EBIT) measurements (used for calibrating resonance energies), have been carried out for the inner-shell $1s \rightarrow 2\ell$ transitions in He-like and Li-

like nitrogen ions (Beiersdorfer et al. 1999), Li-like, Be-like, B-like and C-like oxygen ions (Schmidt et al. 2004; Gu et al. 2005). In EBIT experiments, the spectrum is contaminated and blended with ions in multiple stages of ionization, making spectral interpretation fraught with difficulties. Cleaner, higher-resolution spectra are obtained at synchrotron radiation facilities; ALS, BESSY II, SOLEIL, ASTRID II and Petra III. EBIT experiments have the advantage of the production of pure ground state populations of atoms or ions, extremely difficult to make with merged beams methods, routinely used at synchrotron radiation facilities.

Photoionization and photoabsorption cross sections used for the modelling of astrophysical phenomena has traditionally been provided by theory, as limited experimental data is available across a wide range of wavelengths. Until recently, the bulk of theoretical work has not been tested thoroughly by experiment (McLaughlin 2001; Mueller et al. 2010; Foster et al. 2010; Gharaibeh et al. 2011; Sant’Anna et al. 2011). For atomic oxygen the availability of x-ray data on this system provided the motivation to perform theoretical *K*-shell photoionization investigations.

Inner-shell excitation processes occurring with the interaction of a photon on the $1s^2 2s^2 2p^4 \ ^3P$ ground-state of atomic oxygen produces strong resonances observed in the corresponding cross section (c.f., Figure 2 and Table 1), through promotion of the $1s \rightarrow np$ electron via the processes;

$$h\nu + O(1s^2 2s^2 2p^4 \ ^3P) \rightarrow O(1s 2s^2 2p^4 \ [^2,^4P]np \ ^3P^\circ)$$

giving competing decay routes namely,

$$O^+ (1s^2 2s^2 2p^3 \ [^4S^\circ, ^2D^\circ, ^2P^\circ]) + e^-(k_\ell^2),$$

and

$$O^+ (1s^2 2s^2 2p^2 \ [^3P, ^1D, ^1S])n'\ell' + e^-(k_\ell^2),$$

which the present theoretical approach attempts to simulate, where, $n = 2 - 6$ (observed in the experiment), and k_ℓ^2 is the outgoing energy of the continuum electron with angular momentum ℓ . *K*-shell photoionization contributes to the ionization balance in a more complicated way than outer shell photoionization. *K*-shell photoionization when followed by Auger decay couples three or more ionization stages instead of two in the

usual equations of ionization equilibrium (Petrini & de Araújo 1994, 1997).

Early theoretical photoionization (PI) cross section calculations for K -shell processes on this complex performed by Reilman and Manson (Reilman & Manson 1979) used the Hartree-Slater wavefunctions of Herman and Skillman (Herman & Skillman 1963; Yeh 1993) and the Dirac-Slater wavefunctions (Verner et al. 1993). Photoionization cross sections determined from central field approximations although excellent for high photon energies yield unreliable results near thresholds (see Figure 3 (a)), where resonance features dominate the cross sections (Yeh 1993; Gharaibeh et al. 2011).

State-of-the-art *ab initio* calculations for photoabsorption cross-sections and Auger inner-shell processes were first investigated on this system, using the standard R-matrix approach (McLaughlin & Kirby 1998), for modelling the resolved interstellar O K , Ne K , and Fe L -edge absorption spectra in the *Chandra* x-ray Observatory Low-Energy Transmission Grating Spectrometer (LETGS) spectrum of the low-mass x-ray binary X0614+091 (Paerels et al. 2001). This work was extended using the optical potential technique (Gorczyca & McLaughlin 2000) to account for Auger broadening of resonances below the $1s^{-1}$ threshold and to analyze the high-resolution spectroscopy of the oxygen K -shell interstellar absorption edge in seven x-ray binaries (Juett et al. 2004). Garcia and co-workers (Garcia et al. 2005), using the optical potential method within the Breit-Pauli R-matrix formalism (Burke 2011) extended this work to the oxygen iso-nuclear sequence and to investigate the x-ray absorption structure of atomic oxygen in the interstellar medium by analyzing *XMM-Newton* observations of the low-mass x-ray binary Sco X-1 (Garcia et al. 2011).

2. Experiment

Cross sections for atomic oxygen K -shell photoionization were measured over the photon range 520 eV to 555 eV. Our new results were obtained on undulator beamline 11.0.2 at the ALS, previous measurements were performed on bend-magnet beamline 6.3.2 (Stolte et al. 1997). The present experimental measurements have covered the com-

plete K -shell region, in a single scan, rather than constructing the spectra piece-meal like as was done previously (Stolte et al. 1997). A resolution of 4250 ± 400 ($\approx 124 \pm 12$ meV) at 526.8 eV, and a photon flux of over 10^{11} photons/s was provided by BL 11.0.2 when using slit widths of 20 μ m. The experimental apparatus has been discussed previously in detail (Angel & Samson 1980; Stolte et al. 1997, 2008).

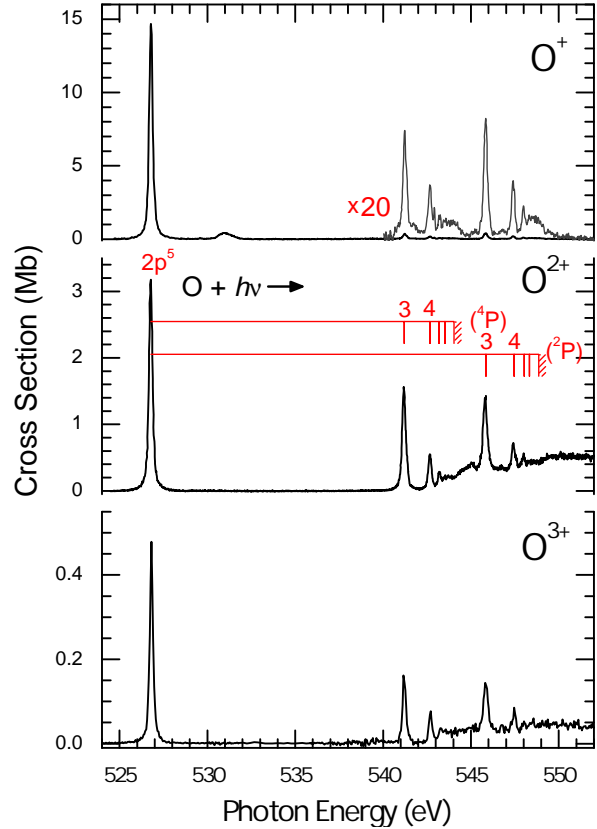


Fig. 1.— (Colour online) Photoionization cross sections of O^+ , O^{2+} and O^{3+} produced by the decay of a $1s$ hole in atomic oxygen. The resonance lines represent the transitions $1s2s^22p^5(^3P^o)$, $1s2s^22p^4(^4P)np$ and $1s2s^22p^4(^2P)np$ with $n = 3 - 6$. The current resolving power of the monochromator was 4250 ± 400 ($\approx 124 \pm 12$ meV) at a photon energy of 526 eV.

Similar to our earlier results (Stolte et al. 1997), we used the Rydberg resonance features found in molecular oxygen near 541 eV to calibrate the photon energy scale, resulting in a maximum uncer-

tainly of 40 meV. During double-bunch operations of the ALS, a Wiley-McLaren style time-of-flight mass spectrometer (Wiley & McLaren 1955), oriented with its axis parallel to the polarization vector of the incident synchrotron radiation, was used in conjunction with a microwave discharge system to determine the branching ratios for atomic oxygen at the $1s2s^22p^5$ ($^3P^\circ$) resonance.

Both the microwave *on* (O and O₂ mixture) and *off* (O₂) independent spectral scans were divided by the incident photon flux. The molecular contribution to the microwave *on* spectrum was removed by a scaled subtraction of a microwave *off* spectrum at the O₂ : $1s \rightarrow 1\pi_g^*$ resonance (530.5 eV). Several residual peaks are created due to the molecular resonances being a few meV wider for the microwave *on* spectra. We surmise this difference is probably due to the larger thermal motion of the gas molecules with the microwave discharge on. The scans were finally corrected by removal of the background produced by direct photoionization of the atomic oxygen valence shell. This was only necessary for O⁺ or O²⁺, being that O³⁺ sat on a zero background. We performed two coarse photon energy scans, one for each ion, covering the range between 500 – 600 eV. The O⁺ or O²⁺ signal produced by *K*-shell photoionization is superimposed on a nearly flat background caused by direct photoionization of the valence shell. This background contributed 35% and 8% to the total O⁺ and O²⁺ signals, respectively, just above the $1s^{-1} 2P$ series limit. The independent ion specific photon energy scans could then be placed onto a relative scale by using the branching ratios (O⁺/TIY = 80.07%, O²⁺/TIY = 17.32%, and O³⁺/TIY = 0.026%, with TIY = total ion yield) measured with the time-of-flight mass analyzer on top of the $1s2s^22p^5$ (3P) resonance. Finally, the scans were placed onto an absolute scale (see Figure 1) by summing their values above the 2P ionization limit and normalizing this sum to the difference of the cross sections above and below the oxygen *K*-edge (Stolte et al. 1997, 2008).

3. Theory

The *R*-matrix with pseudo-states method (Burke 2011; Berrington et al. 1995; Robicheaux et al. 1995; Ballance & Griffin 2006) was used to determine our theoretical results. Cross section

calculations were performed in *LS*-coupling retaining 910-levels (valence and hole-states) of the residual O⁺ ion in the close-coupling expansion. Hartree-Fock 1s, 2s and 2p (Clementi & Roetti 1974) and *n*=3 pseudo-orbitals of the O⁺ residual ion (included for core relaxation and correlations effects) were used, obtained by optimizing on the energy of the hole state; $\overline{3s}$, $\overline{3p}$ and $\overline{3d}$ on $1s2s^22p^4$ 4P including the important configuration $1s^22s^22p^2\overline{3d}$ 4P with the multi-configuration-Hartree-Fock (MCHF) atomic structure code (Fischer 1991).

For the O($1s^22s^22p^4$ 3P) bound state we obtained 14.0344 eV for the ionization potential using a triple electron promotion model, the NIST experimental value is 13.61806 eV, a discrepancy of ~ 3 %, or 416 meV. A double electron promotion model gave 13.82184 eV, a discrepancy of ~ 1.5 %, or 204 meV, yielding closer agreement with the NIST tabulated value as the RMPS approach provides more highly correlated wave functions. In previous work (Gorczyca & McLaughlin 2000) obtained an underestimate of the ionization potential ~ 2.5 %, or 338 meV compared to experiment, due to limited correlation included.

In the collision calculations for atomic oxygen, twenty continuum functions and a boundary radius of 7.27 Bohr radii was used. Two and three-electron promotion scattering models were investigated giving similar results. The collision problem was solved using an energy grid of 2×10^{-7} Rydbergs (≈ 2.72 μ eV) allowing detailed resolution of resonance features in the cross sections.

The peaks found in the photoabsorption cross section spectrum were fitted to Fano profiles (Fano & Cooper 1968) instead of the energy derivative of the eigenphase sum technique (Quigley et al. 1998; Ballance et al. 1999). Theoretical values for the natural linewidths Γ (meV) are presented in Table 1 and compared with current and previous ALS measurements (Stolte et al. 1997) and with prior investigations.

4. Results and Discussion

In the photon energy range (520 eV – 555 eV) explored, intense structure is observed in the cross section between 520 eV and 530 eV, from the strong $1s \rightarrow 2p$ transition in the atomic oxygen spectrum. Figure 2 shows our present experimen-

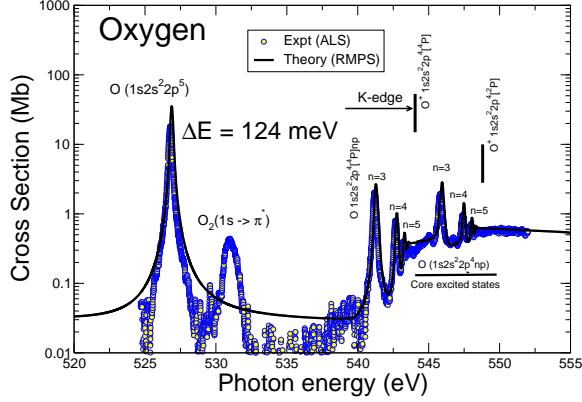


Fig. 2.— (Colour online) Atomic oxygen photoabsorption cross sections taken at 124 meV FWHM compared with theoretical estimates. The R-matrix calculations shown are from the RMPS method (solid black line, present results) convoluted with a Gaussian profile of 124 meV FWHM. Table 1 designates the resonances and their properties.

tal and theoretical results for the photon energy range of 520 eV – 555 eV illustrating all the additional $1s \rightarrow np$ transitions ($n \geq 3$) in the spectrum. Previous experimental measurements (Stolte et al. 1997) were actually measured at a photon energy resolution of 135 meV and not 182 meV, current ALS measurements are at 124 meV FWHM. Convolution of the RMPS theoretical results with a Gaussian function of 124 meV FWHM was used to compare directly with the ALS measurements. Resonances observed in the experimental measurements were fitted with Voigt profiles to determine the natural linewidths using a Gaussian function of 124 meV FWHM for each peak. The photon energy was calibrated to an energy uncertainty of approximately ± 40 meV.

Previous measurements of Stolte and co-workers (Stolte et al. 1997) were re-analyzed with the present results. The measured spectra for O^+ , O^{2+} and O^{3+} production were fitted with the program WinXAS[©] of Thorsten Ressler, Hamburg, Germany (Ressler 1983) and its near edge x-ray absorption fitting routines. Due to an in-

complete data set, previous measurements for O^{3+} (Stolte et al. 1997) were not fitted. In previous measurements (Stolte et al. 1997), a width of 231 meV was cited with a resolution of 182 meV. On refitting the previous results (Stolte et al. 1997) it was discovered that it was not possible to arrive at a proper fit with a resolution of 3000. Current multi-function fits, using Voigt and arctan functions, determined the resolution to be 3800 ± 150 ($\approx 135 \pm 5$ meV). The $1s2s^2 2p^4(^4P^e)6p$ and $1s2s^2 2p^4(^2P^e)6p$ states cannot be properly fitted, since they are completely hidden.

Rydberg’s formula was used to determine the resonance energies, given by,

$$\epsilon_n = \epsilon_\infty - \frac{Z^2}{\nu^2}. \quad (1)$$

Where, ϵ_n is the resonance transition energy, in Rydbergs, ϵ_∞ the ionization potential and the resonance series limit. The principal quantum number n , the effective quantum number ν and the quantum defect μ are related by $\nu = n - \mu$ (Seaton 1983; Hinojosa et al. 2012). Converting all quantities to eV, members of the Rydberg series are represented by,

$$E_n = E_\infty - \frac{Z^2 \mathcal{R}}{(n - \mu)^2}. \quad (2)$$

E_n is the resonance energy position, E_∞ the ionisation limit, Z is the charge of the core (in this case, $Z = 1$) and \mathcal{R} is 13.6057 eV (Seaton 1983; Hinojosa et al. 2012).

In Figure 2 we present the experimental cross section measurements from the ALS taken at 4250 ± 400 ($\approx 124 \pm 12$ meV) resolution compared to our theoretical work. In the non-resonant region, above the K edge, at 550 eV, theory gives a value of 0.560 Mb, the ALS experimental measured value is 0.559 Mb, a discrepancy of 0.03%. Figure 2 shows the excellent agreement between theory and experiment over the entire energy region and Figure 3 (a) illustrates the RMPS results with the central field approximation (Yeh 1993) results. Strong resonance features near the K-edge present in the state-of-the-art RMPS cross sections are absent from the central field calculations. In Figure 3(b) un-convoluted, RMPS cross sections with the optical potential R-matrix results (Gorczyca & McLaughlin 2000) are presented. Note, the discontinuity (~ 538 eV) in the

optical potential R-matrix cross section results absent from the RMPS calculations. Finally, Figure 4 compares quantum defects μ obtained from the RMPS and the optical potential methods (Gorczyca & McLaughlin 2000; Garcia et al. 2005) with experiment.

Table 1 presents our experimental and theoretical results, for resonance energies, resonance strengths $\bar{\sigma}_{n\ell}$ (Mb eV), quantum defects μ and natural linewidths Γ (meV) with previous theoretical and experimental work (Stolte et al. 1997; Petrini & de Araújo 1994; Menzel et al. 1996; Saha 1994; Krause 1994). Table 1 includes the experimental values for the lifetime τ expressed in femtoseconds (fs), determined via the uncertainty principle ($\Delta E \Delta t = \hbar/2$).

5. Conclusions

K-shell photoabsorption of atomic oxygen was investigated using the R-matrix with pseudo-states (RMPS) method along with current and previous high resolution experimental measurements made at the ALS. Resonance features observed in the cross sections for photon energies in the range 520 eV – 555 eV, are identified as $1s \rightarrow np$ transitions that are analyzed, natural linewidths Γ (meV) extracted and lifetimes determined via the uncertainty principle. Excellent agreement (see Table 1) of theoretical estimates, for the resonance parameters (resonance energies, natural line widths and quantum defects) compared to experimental measurements is obtained with calculations for the ionization potential accurate to within 1.5 % of experiment. We have delineated *all* of the resonances properties and made a detailed comparison of experiment with current and previous theoretical investigations. Earlier theoretical work (Gorczyca & McLaughlin 2000; Garcia et al. 2005) made a limited comparison with experiment, for the quantum defects of the two resonance series with only the Auger width of $1s2s^22p^5\ ^3P^\circ$ state determined. The present ALS high resolution (124 meV FWHM) of all the resonance peaks observed in the cross sections over the *entire* energy range investigated allowed a direct comparison with state-of-the-art R-matrix calculations to be made. The only limitation of the present theoretical model is apparent from Table 1 concerning the resonance strengths

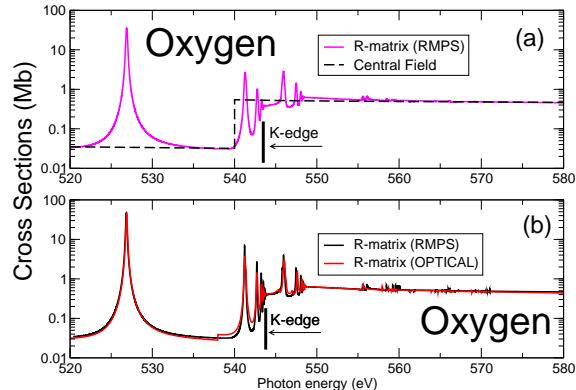


Fig. 3.— (Colour online) (a) R-matrix (RMPS) cross sections (convolved at 124 meV) compared with central field approximation results (Yeh 1993), (b) Cross sections (unconvolved) from the RMPS (solid black line) and Optical Potential R-matrix calculations (solid red line).

which might be addressed in the future with an extended pseudo-states basis within a Breit-Pauli approximation. Finally, the data is suitable to be incorporated into the astrophysical modelling codes CLOUDY (Ferland 2003), XSTAR (Kallman & Bautista 2001) and AtomDB (Foster et al. 2012).

The energy resolution on present day satellites, *Chandra* and *XMM-Newton*, is ~ 0.6 eV, a factor of 10 lower than available at current ground based synchrotron radiation facilities, like the ALS, SOLEIL, ASTRID II, BESSY II or PETRA III, providing higher resolution and precision than obtained via satellites. There are also issues concerning the calibration of spectra obtained from satellites as previously highlighted. The ALS measurements have been calibrated to the resonance transition in molecular oxygen, which is known very accurately.

In contrast to this, observed spectra using the LETG on *Chandra*, are calibrated to either theoretical calculations or EBIT measurements (Schmidt et al. 2004; Gu et al. 2005) for the $1s \rightarrow 2p$ resonance line in H-like, He-like oxygen, Li-like or B-like oxygens ions (with all the ensuing

TABLE 1

THEORY AND EXPERIMENT VALUES FOR THE RESONANCE PARAMETERS FOR THE $1s2s^22p^5(^3P^\circ)$ AND $1s2s^22p^4(^2,^4P)np\ ^3P^\circ$, RYDBERG SERIES ($n \geq 3$) CONVERGING TO THE $1s^{-1}\ ^4P$ AND $1s^{-1}\ ^2P$ SERIES LIMITS OF ATOMIC OXYGEN.

Resonances (Symmetry)	Energy (eV)	Energy (eV)	μ	μ	Γ (meV)	Γ (meV)	Lifetime τ (fs)
Label ($^3P^\circ$)	Theory (R-matrix ^a)	Expt (ALS ^b)	Theory (R-matrix ^a)	Expt (ALS ^b)	Theory (R-matrix ^a)	Expt (ALS ^b)	Expt (ALS ^b)
$2p^5$	526.83	526.79 ± 0.04	1.110	1.110 ± 0.003	150^a 169^e 139^f	148 ± 11^b 153 ± 12^c 160 ± 9^d	2.22 ± 0.17 - -
3p	541.23	541.19 ± 0.04	0.796	0.811 ± 0.023	143	167 ± 11	1.97 ± 0.13
4p	542.70	542.68 ± 0.04	0.801	0.825 ± 0.063	97	125 ± 11	2.63 ± 0.23
5p	543.25	543.23 ± 0.04	0.824	(0.800 ± 0.29)	70	119 ± 10	2.77 ± 0.23
6p	543.52	543.51 ± 0.04	0.833	(0.800 ± 0.29)	80	196 ± 12	1.68 ± 0.10
-	-	-	-	-	-	-	-
$1s^{-1}\ ^4P$	544.03	544.03 ± 0.04	-	-	-	-	-
3p	545.97	545.83 ± 0.04	0.826	0.870 ± 0.015	187	196 ± 10	1.68 ± 0.10
4p	547.48	547.45 ± 0.04	0.848	0.871 ± 0.045	127	128 ± 10	2.57 ± 0.20
5p	548.04	548.04 ± 0.04	0.902	(0.870 ± 0.105)	102	156 ± 10	2.11 ± 0.14
6p	548.35	548.33 ± 0.04	0.784	(0.870 ± 0.201)	110	157 ± 13	2.10 ± 0.17
-	-	-	-	-	-	-	-
$1s^{-1}\ ^2P$	548.85	548.85 ± 0.04	-	-	-	-	-
Resonance			Strengths Theory (R-matrix ^a)	Strengths Experiment (ALS ^b)			
Series			$\bar{\sigma}_{n\ell}$	$\bar{\sigma}_{n\ell}$			
$1s2s^22p^4(^4P)n\ell\ ^3P^\circ$			(Mb eV)	(Mb eV)			
$\bar{\sigma}_{2p}$			10.22	5.76 ± 1.45			
$\bar{\sigma}_{3p}$			0.88	0.68 ± 0.17			
$\bar{\sigma}_{4p}$			0.30	0.25 ± 0.06			
$\bar{\sigma}_{5p}$			0.13	0.08 ± 0.02			
$\bar{\sigma}_{6p}$			0.09	-			
$1s2s^22p^4(^2P)n\ell\ ^3P^\circ$							
$\bar{\sigma}_{3p}$			1.12	0.58 ± 0.15			
$\bar{\sigma}_{4p}$			0.44	0.17 ± 0.04			
$\bar{\sigma}_{5p}$			0.20	0.07 ± 0.02			
$\bar{\sigma}_{6p}$			0.16	-			

References. — ^aR-matrix (RMPS), $1s^{-1}\ ^2,^4P$ series limit are the ALS measurements of Stolte and co-workers (Stolte et al. 1997); ^bExperiment, resolution of 4250 ± 400 (124 ± 12 meV), to fit the current ALS data; ^cExperiment, resolution of 3800 ± 150 (135 ± 5 meV), to refit the previous ALS data (Stolte et al. 1997); ^dExperiment, Wisconsin, Synchrotron Radiation Center (SRC), Krause and co-workers (Krause 1994; Menzel et al. 1996); ^eMulti-Configuration-Hartree-Fock (MCHF), Saha (Saha 1994); ^fS-matrix method, Petrini and de Araújo (Petrini & de Araújo 1994). Experimental and theoretical energies (eV), quantum defects μ and natural linewidths Γ (meV), for the two prominent Rydberg series are presented. Lifetimes, τ (fs), given for the resonance states were determined from the uncertainty principle. Bracketed values represent the ALS experimental energies (eV) and quantum defects obtained using an average value of μ . The error in the calibrated photon energy is ± 40 meV. Instrumental resolution of 3800 ± 150 ($\approx 135 \pm 5$ meV) was used for the Gaussian portion of the Voigt function when refitting the previous (Stolte et al. 1997) and 4250 ± 400 ($\approx 124 \pm 12$ meV) for the current ALS experimental data.

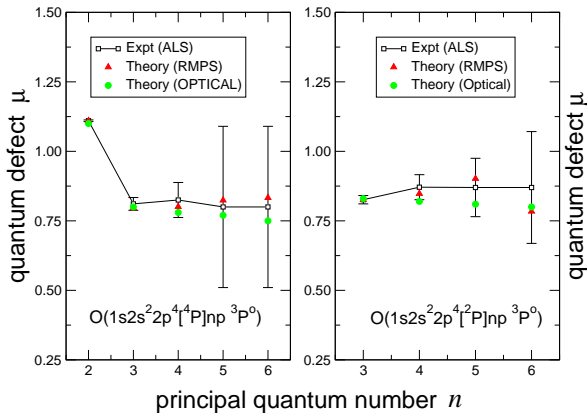


Fig. 4.— (Colour online) ALS experimental quantum defects with those obtained from theory. The RMPS results, filled triangles, solid circles optical potential approach (Gorczyca & McLaughlin 2000; Garcia et al. 2005).

complications and difficulties of ion identification). Given the high precision of our experimental and theoretical data we recommend that observational data concerning *K*-shell photoabsorption of atomic oxygen be calibrated to the present work.

BMMcL, and CPB thank the Institute for Theoretical Atomic and Molecular Physics (ITAMP), at the Harvard-Smithsonian Center for Astrophysics for their hospitality and support (BMMcL) under the visitor's program. ITAMP is supported by a grant from the National Science Foundation. CPB acknowledges support by US Department of Energy (DoE) grants through Auburn University. WCS acknowledges support from the National Science Foundation under NSF Grant No. PHY-01-40375. We thank Professor Alex Dalgarno FRS, Dr John C Raymond, Dr Randall K Smith, Dr Jeremy J Drake and Dr Brad Wargelin for discussions on the astrophysical applications and the LETG *Chandra* calibration. Grants of computational time at the National Energy Research Scientific Computing Center in Oakland, CA, USA, the Kraken XT5 facility at the National Institute for Computational Science (NICS) in Knoxville, TN, USA and at the High Performance Comput-

ing Center Stuttgart (HLRS) of the University of Stuttgart are gratefully acknowledged. The Kraken XT5 facility is a resource of the Extreme Science and Engineering Discovery Environment (XSEDE), which is supported by National Science Foundation Grant No. OCI-1053575. The help of Hendrik Blum and Tolek Tyliczszak in setting up the experiment on beamline 11 at the ALS is gratefully acknowledged. The Advanced Light Source in Berkeley, CA, USA, is supported by the Director, Office of Science, Office of Basic Energy Sciences, of the US Department of Energy under Contract No. DE-AC02-05CH11231.

REFERENCES

- Angel, G. C., & Samson, J. A. R. 1980, *Phys. Rev. A*, 38, 5578
- Ballance, C. P., & Griffin, D. C. 2006, *J. Phys. B At. Mol. & Opt. Phys.*, 39, 3617
- Ballance, C. P. et al. 1999, *Phys. Rev. A*, 60, R4217
- Beiersdorfer, P. et al. 1999, *Rev. Sci. Instrum.*, 70, 276
- Berrington, K. A. et al. 1995, *Comput. Phys. Commun.*, 92, 290
- Burke, P. G. 2011, *R-Matrix Theory of Atomic Collisions Application to Atomic, Molecular and Optical Processes* (New York, USA: Springer)
- Clementi, E., & Roetti, C. 1974, *At. Data Nucl. Data Tables*, 14, 177
- Costantini, E. et al. 2012, *A&A*, 539, A32
- Fano, U., & Cooper, J. W. 1968, *Rev. Mod. Phys.*, 40, 441
- Ferland, G. J. 2003, *ARA&A*, 41, 517
- Fischer, C. F. 1991, *Comput. Phys. Commun.*, 64, 369
- Foster, A. R. et al. 2010, *Space Sci. Rev.*, 157, 135
- . 2012, *ApJ*, 756, 128
- Garcia, J. et al. 2005, *ApJS*, 158, 68

- . 2009, *ApJS*, 185, 477
- . 2011, *ApJ*, 731, L15
- Gharaibeh, M. F. et al. 2011, *J. Phys. B At. Mol. & Opt. Phys.*, 44, 175208
- Gorczyca, T. W., & McLaughlin, B. M. 2000, *J. Phys. B At. Mol. & Opt. Phys.*, 33, L859
- Gu, M. F. et al. 2005, *ApJ*, 627, 1066
- Hasoglu, M. F. et al. 2010, *ApJ*, 724, 1296
- Herman, F., & Skillman, S. 1963, *Atomic Structure Calculations* (Englewood Cliffs, NJ, USA: Prentice-Hall)
- Hinojosa, G. et al. 2012, *Phys. Rev. A*, 44, 175208
- Juett, A. M. et al. 2004, *ApJ*, 612, 308
- Kallman, T. R., & Bautista, M. A. 2001, *ApJS*, 134, 139
- Krause, M. O. 1994, *Nucl. Instr. & Meth. in Phys. Res. B*, 87, 178
- Masuoka, T., & Samson, J. A. R. 1980, *J. Chem. Phys.*, 77, 623
- McLaughlin, B. M. 2001, in *ASP Conf. Series*, Vol. 247, *Spectroscopic Challenges of Photoionized Plasma*, ed. G. J. Ferland & D. W. Savin (San Francisco, CA: Astronomical Society of the Pacific), 87
- McLaughlin, B. M., & Ballance, C. P. 2013, in *McGraw-Hill Yearbook of Science and Technology 2013*, ed. McGraw-Hill (New York, USA: McGraw-Hill Inc), 281
- McLaughlin, B. M., & Kirby, K. P. 1998, *J. Phys. B At. Mol. & Opt. Phys.*, 31, 4991
- Menzel, A. et al. 1996, *Phys. Rev. A*, 54, R991
- Miyake, S. et al. 2010, *ApJ*, 709, L168
- Mueller, A. M. et al. 2010, *J. Phys. B At. Mol. & Opt. Phys.*, 43, 135602
- Paerels, F. et al. 2001, *ApJ*, 546, 338
- Petrini, D., & de Araújo, F. X. 1994, *A&A*, 282, 315
- Petrini, D., & de Araújo, F. X. 1997, *A&A*, 326, 870
- Quigley, L. et al. 1998, *Comput. Phys. Commun.*, 114, 225
- Reilman, R. F., & Manson, S. T. 1979, *ApJS*, 40, 85
- Ressler, T. 1983, *J. Synchrotron Rad.*, 5, 118
- Robicheaux, F. et al. 1995, *Phys. Rev. A*, 52, 1319
- Saha, H. P. 1994, *Phys. Rev. A*, 49, 894
- Sant’Anna, M. M. et al. 2011, *Phys. Rev. Lett.*, 107, 033001
- Schmidt, M. et al. 2004, *ApJ*, 604, 562
- Seaton, M. J. 1983, *Rep. Prog. Phys.*, 46, 167
- Skinner, S. L. et al. 2010, *AJ*, 139, 825
- Stancil, P. C. et al. 2010, in *Proceedings of the Dalgarno Celebratory Symposium*, ed. J. F. Babb, K. Kirby and H. Sadeghpour (London, UK: World Scientific Imperial College Press), 102
- Stolte, W. C. et al. 1997, *J. Phys. B At. Mol. & Opt. Phys.*, 30, 4489
- . 2008, *J. Phys. B At. Mol. & Opt. Phys.*, 41, 145102
- Verner, D. A. et al. 1993, *At. Data Nucl. Data Tables*, 55, 233
- Wiley, W. C., & McLaren, I. H. 1955, *Rev. Sci. Inst.*, 26, 1050
- Yeh, J. 1993, *Atomic Calculation of Photoionization Cross-Sections and Asymmetry Parameters* (New York, USA: Gordon & Breach)